Applied Mathematics and Computation 495 (2025) 129301

Contents lists available at ScienceDirect

Applied Mathematics and Computation

journal homepage: www.elsevier.com/locate/amc

Computational aspects of hyperbolic curvature flow

Monika Suchomelová, Michal Beneš *, Miroslav Kolář

Department of Mathematics, Faculty of Nuclear Sciences and Physical Engineering, Czech Technical University in Prague, Trojanova 13, Prague, 12000, Czech Republic

ARTICLE INFO

MSC:
primary 35L20, 35L80, 53Z05, 65M08
secondary 74N20

Keywords:
Curvature driven flow
Parametric curve description
Hyperbolic curvature flow
Flowing finite-volume method

ABSTRACT

The article analyzes behavior of the solution of the hyperbolic curvature flow by means of a class of analytical solutions and by computational studies performed by a semi-discrete finite-volume scheme. A class of analytical solutions is derived and used for the verification of the computational algorithm by numerical convergence to it. An original tangential redistribution is proposed to stabilize the numerical scheme. Its derivation requires a four-dimensional transformation of the evolution law. The role of tangential redistribution is demonstrated on computational examples. Computational studies show evolution of the initially convex and non-convex curves, and include cases when singularities predicted by theory start to develop.

1. Introduction

This article focuses on the motion of curves in plane where the acceleration is given by curvature in the sense specified below. This type of motion can be called the hyperbolic (mean) curvature flow as the acceleration is expressed by the second time derivative of position, and can be phrased as

$$\text{acceleration} + \text{dissipation} = \text{curvature} + \text{forces}. \tag{1}$$

The curvature term in (1) contributes, due to the line tension, to forces acting on the curve. The dissipation term in (1) is given by the velocity. If the acceleration is negligible with respect to other terms, the dissipation in terms of the velocity prevails on the left-hand side, recovering the well-known dissipative curvature flow

$$\text{velocity} = \text{curvature} + \text{forces}, \tag{2}$$

which is, due to its wide application range, mostly studied in literature (we refer the reader to theoretical results in [15,16,1,10], numerical solution in [11,14,42], applications in [5,7,28,6], and to more references therein).

Below, we present a motivation and historical overview of literature introducing and analyzing motion law (1). Originally, motion law (1) was motivated by laboratory experiments with helium at temperatures close to the absolute zero and at high pressure where the growing helium crystals exhibited melting-freezing crystallization waves, as described in [2,27]. Using principles of continuum mechanics and thermodynamics, motion law of the type (1) was formulated in [20,21] for the crystallization waves in solid-liquid phase transitions. The same type of motion law was derived for dynamics of thin liquid film or foam dynamics within the gas-liquid

* Corresponding author.
E-mail address: michal.benes@fjfi.cvut.cz (M. Beneš).

https://doi.org/10.1016/j.amc.2025.129301
Received 7 July 2024; Received in revised form 31 December 2024; Accepted 14 January 2025

two-phase fluid flow, first in [25], then in [26]. In [24], this approach to modeling foams and thin films was confirmed. The same motion law applied to a vibrating membrane was suggested in [51].

Based on the above mentioned applications, [40] studied the damped version of motion law (1) of a closed simple curve γ written as

$$v_\gamma^{\cdot} + \delta v_\gamma = \kappa_\gamma, \tag{3}$$

in the direction of the inner normal vector where $\delta > 0$, κ_γ is the curvature, v_γ is the normal velocity, and $v_\gamma^{\cdot}$ is the normal acceleration defined as the time derivative of the normal velocity v along a path normal to the γ. In [40], evolution law (3) was formulated in an anisotropic version as well, and it was studied numerically by means of a crystalline algorithm. In [41], the authors considered a hyperbolic phase-field model, from which a version of (3) with nonlinear damping was obtained by the asymptotic analysis.

As for the dissipative motion law (2), the parametric method is convenient in analyzing and solving motion law (1). For this purpose we identify the notation for the curve γ with its parametrization $\gamma = \gamma(t, s)$ where t is the time, and s is the arc-length parameter. Using the Frenet frame $\vec{T}, \vec{N}$, Yau in [51] formulated the hyperbolic version of mean curvature flow of hypersurfaces, which, in plane, has the form

$$\partial_{tt}\gamma = \kappa_\gamma \vec{N}. \tag{4}$$

However, this flow is not normal, even when the initial velocity is in the normal direction. Motion law (4) was analyzed more in [23] from the view point of formulation, local existence and uniqueness, analytical solution in simple situations, and nonlinear stability.

Independently, a geometric evolution equation for hypersurfaces was derived in [32] based on the conservation of momentum. The Hamiltonian principle was used on actions containing kinetic and internal energy. In plane, this motion law reads

$$\partial_{tt}\gamma = \frac{1}{2}(1 + |\partial_t\gamma|^2)\kappa\vec{N} - \langle \partial_{st}\gamma, \partial_t\gamma\rangle\vec{T}, \tag{5}$$

where $\langle\cdot,\cdot\rangle$ denotes the scalar product in $\mathbb{R}^2$, and the operator ∂_{st} is defined as $\partial_{st} = \partial_s\partial_t$. In this case, the tangential term ensures that (5) is normal provided the initial velocity is normal.

Another article [29] considered an evolution equation for parametric curves and studied blow-up criteria. This motion law applied to planar curves has the form

$$\partial_{tt}\gamma = \kappa\vec{N} - \langle \partial_{st}\gamma, \partial_t\gamma\rangle\vec{T}. \tag{6}$$

The flow can be called hyperbolic curve shortening flow as an analogue to classic curve shortening flow.

The assumptions in the mentioned article involved convexity of the initial curve and the normal initial velocity, i.e. the initial velocity in the form $v_0\vec{N}_0$ where $\vec{N}_0$ is the normal vector of the initial curve. The tangential term again ensures that the flow is normal. Motion law (6) is subject of this article.

In subsequent papers on this subject, [30] studied singularities for evolving closed convex curves, whereas [45] discussed singularities for the hyperbolic mean curvature flow in a Minkowski space. The article [22] analyzed self-similar solutions of one-dimensional flow (6). The authors of [49] added the dissipation term to (6) as in (1) and (3). Variety of forcing terms for (1) were considered in [33,46,47]. Motion law (1) has been generalized in different ways for the affine invariant curve flow in [50], for the hyperbolic power mean curvature flow in [52], for the Gauss curvature in [9], the inverse mean curvature in [34,48]. Recently, [17,18] studied symmetries and conservation laws for the hyperbolic motion by mean curvature, [8] analyzed normal flow, [35] provided representation formulae for it.

Numerical solution of motion law (1) is so far presented in few articles - the crystalline approach was used in [40], the HMBO algorithm was used in [19,31], the level-set method and ENO schemes in [26], and the fully discrete three-level finite-difference scheme with constant time step was used in [12] to solve the parametric formulation of (1).

In this paper, we summarize properties of evolution equation (6), derive the analytical solution under specific conditions, serving as benchmarks for verification of the numerical algorithm. It is based on a semi-discrete scheme based on the finite-difference approximation of the parametric evolution law. The resulting system of ODE's is then solved in time by a higher-order time solver with adaptive time step. This scheme is used to conduct computational studies of the hyperbolic curvature flow for a variety of initial conditions. Performance of the numerical algorithm is improved by means of an original redistribution of discretization points derived by means of a four-dimensional variant of the motion law.

The article is therefore structured in four sections beyond Introduction. In Section 2, main analytical properties of evolution equation (6) are summarized. This motion law is modified to allow for a suitable redistribution along the curve without disturbing the curve motion. Analytical solution of (6) is studied in Section 3. In Section 4, we derive semi-discrete numerical schemes and describe the numerical algorithm. Finally, Section 5 contains comparison with the analytical solution, examples of evolution for various initial conditions and including the redistribution effects.

2. Mathematical properties of the flow

First, we formulate the motion law (6) in more detail. Let the closed curve γ be parametrized by a parameter $u \in [0, 1]$. We say that γ is immersed provided $|\partial_u\gamma| \neq 0$. For such a curve, the Frenet frame, i.e. tangent and normal vector, is defined correctly.

For the purpose of reformulating the motion law (6), we express the tangent vector $\vec{T}$ and the normal vector $\vec{N}$ by means of the parametrization and using the arc-length variable s for which $\partial_s = |\partial_u\gamma|^{-1}\partial_u$:

$$\vec{T} = \partial_s\gamma, \quad \vec{N} = \partial_s\gamma^{\perp}.$$

Here, the symbol $^{\perp}$ is defined for any two-dimensional vector $\vec{v} = (v_1, v_2)$ as $\vec{v}^{\perp} = (-v_2, v_1)$. Together with the Frenet equation $\partial_s\vec{T} = \kappa\vec{N}$ we express the term $\kappa\vec{N}$ using the parametrization:

$$\kappa\vec{N} = \frac{1}{|\partial_u\gamma|}\partial_u\left(\frac{\partial_u\gamma}{|\partial_u\gamma|}\right).$$

From (6), we obtain the **Evolution problem 1** for the parametric curve $\gamma : S^1 \times [0,T) \to \mathbb{R}^2$ which has the form of a system of non-linear partial differential equations

$$\begin{aligned} \partial_{tt}\gamma &= \frac{1}{|\partial_u\gamma|}\partial_u\left(\frac{\partial_u\gamma}{|\partial_u\gamma|}\right) - \frac{1}{|\partial_u\gamma|^2}\langle\partial_{ut}\gamma, \partial_t\gamma\rangle\partial_u\gamma \quad && \text{in } S^1\times(0,T), \\ \gamma|_{t=0} &= \gamma_0 && \text{in } S^1, \\ \partial_t\gamma|_{t=0} &= \gamma_1 && \text{in } S^1. \end{aligned} \tag{7}$$

Here γ_0 is the initial closed curve and γ_1 is the initial velocity. We assume that the initial curve is smooth and immersed. In addition, we demand the initial curve to be embedded, i.e. not intersecting itself. Even though the system of equations is non-linear, it can be proved that they form a quasi-linear system of PDEs as the right-hand sides can be expresses as linear combinations of the second-order derivatives of the parametrization components by expressions containing lower-order derivatives - see also [44].

Curve flow (7) was studied in [29], specifically for smooth strictly convex initial curve and the normal initial velocity in form $\gamma_1 = v_0\vec{N}_0$ where $\vec{N}_0$ stands for the normal vector of the initial curve. For the function $v_0 = v_0(u)$, the authors required that $v_0 \geq 0$. They described a convex curve in terms of the support function which led to a single Monge-Ampère equation. Using this formulation, useful properties of flow (7) were proved such as the solution existence on finite time interval, during which the curve shrinks to a point, or converges to a piece-wise smooth curve. In the article, they also proved that evolving curves stay convex during evolution and satisfy the containment principle. The containment principle guaranties the preservation in time of mutual position of two convex curves where one is contained in the interior of another one initially, provided some conditions for the initial velocity are satisfied.

Such a knowledge on asymptotic behavior of the solution is interesting for numerical solution as well, as we can expect a smooth curve to develop singularities in finite time.

Other results, such as convexity preservation and the containment principle can be demonstrated on numerically computed examples as well.

Proposition 1. *For a normal initial velocity, the **Evolution problem 1** is normal.*

Proof. We use the definition of normal flow as mentioned in [9]. We differentiate the term $\langle\partial_t\gamma, \partial_u\gamma\rangle$ with respect to time, use motion law (6) and the facts that $\partial_{tu} = \partial_{ut}$, and $\partial_s = |\partial_u\gamma|^{-1}\partial_u$:

$$\begin{aligned} \frac{\partial}{\partial t}\langle\partial_t\gamma, \partial_u\gamma\rangle &= \langle\partial_{tt}\gamma, \partial_u\gamma\rangle + \langle\partial_t\gamma, \partial_{tu}\gamma\rangle \\ &= |\partial_u\gamma|\langle\kappa\vec{N} - \langle\partial_{st}\gamma, \partial_t\gamma\rangle\vec{T}, \vec{T}\rangle + \langle\partial_t\gamma, \partial_{tu}\gamma\rangle \\ &= -|\partial_u\gamma|\langle\partial_{st}\gamma, \partial_t\gamma\rangle + \langle\partial_t\gamma, \partial_{tu}\gamma\rangle \\ &= -\langle\partial_{ut}\gamma, \partial_t\gamma\rangle + \langle\partial_t\gamma, \partial_{tu}\gamma\rangle = 0. \end{aligned}$$

Therefore, term $\langle\partial_t\gamma, \partial_u\gamma\rangle$ remains constant in time and the tangential velocity

$$\frac{1}{|\partial_u\gamma|}\langle\partial_t\gamma, \partial_u\gamma\rangle$$

is zero provided the initial velocity is in the normal direction. □

In [9], the normal flows were suggested as a special type of flows prescribing the acceleration of the evolving curve which, in the graph formulation, can be reduced to one quasi-linear partial differential equation for one coordinate.

2.1. Redistribution along the curve

Controlling the redistribution of points without affecting the shape of the evolving curve is important for numerical solution of the motion law, especially in applications. For the parabolic curvature flow, corresponding tools exist, as mentioned, e.g. in [36,38,37]. For the hyperbolic flow, a straightforward adding a tangential term to the evolution law is impossible as the law works with accelerations. We therefore rewrite evolution law (7) as a system of first-order equations in 4D, in fact.

Denoting $\eta = \partial_t \gamma$, system (7) can be rewritten as a system of four PDEs

$$\partial_t \begin{pmatrix} \gamma \\ \eta \end{pmatrix} = \begin{pmatrix} \eta \\ \kappa_\gamma \vec{N}_\gamma - \frac{1}{|\partial_u \gamma|} \langle \partial_u \eta, \eta \rangle \vec{T}_\gamma \end{pmatrix} \quad \text{in } S^1 \times (0,T) \tag{8}$$

for κ_γ, $\vec{T}_\gamma$, $\vec{N}_\gamma$, the curvature and the Frenet frame of curve γ. In other words, the velocity of a curve in 4D is prescribed. For such a curve, the tangential vector, which we denote by $\vec{\tilde{T}}$, is defined as

$$\vec{\tilde{T}} = \frac{1}{\sqrt{|\partial_u \gamma|^2 + |\partial_u \eta|^2}} \begin{pmatrix} \partial_u \gamma \\ \partial_u \eta \end{pmatrix}.$$

Introducing a given velocity in this direction by the function $\tilde{\alpha}$, we obtain a modification of (8), the **Evolution problem 2** in the form:

$$\begin{aligned} \partial_t \begin{pmatrix} \gamma \\ \eta \end{pmatrix} &= \begin{pmatrix} \eta \\ \kappa_\gamma \vec{N}_\gamma - \frac{1}{|\partial_u \gamma|} \langle \partial_u \eta, \eta \rangle \vec{T}_\gamma \end{pmatrix} + \tilde{\alpha} \vec{\tilde{T}} \quad && \text{in } S^1 \times (0,T) \\ \begin{pmatrix} \gamma \\ \eta \end{pmatrix} |_{t=0} &= \begin{pmatrix} \gamma_0 \\ \gamma_1 \end{pmatrix} && \text{in } S^1. \end{aligned} \tag{9}$$

We intend to choose $\tilde{\alpha}$ in such a way that it accordingly redistributes the points along the curve while ensuring that the solution of equations (8) and (9) are geometrically the same. This means that the curves as trajectories of the solution at the same time moment overlap. This is commented in the following remark.

Remark. The conditions for the geometric equivalence of the evolution laws can be discussed more in detail considering two evolution laws providing parametrizations of the curves expected to overlap. Then an equation for reparametrization can be derived stating the conditions for the geometric equivalence of the evolution laws.

Motivated by the experience with the dissipative flow as in [5,36], we set

$$\tilde{\alpha} = -\partial_u (|\partial_u \gamma|^{-1}) = \left\langle \frac{\partial_{uu} \gamma}{|\partial_u \gamma|^2}, \vec{T}_\gamma \right\rangle,$$

which is known as the de Turck trick - see [10]. The above described step motivates further study as well as search for other possible choices of $\tilde{\alpha}$.

3. Analytical solutions

Below, we summarize the results concerning analytical solvability of hyperbolic law (7). First case when we are able to calculate analytical solution is under the simplifying assumption of radial symmetry of the evolution problem. The behavior of the circle evolution was mentioned for example in [29] but the explicit solution was not provided. In this section, we also derive the analytical solution for special choice of tangential velocity.

3.1. Evolving circle

For hyperbolic equation (7), the evolving circle is a self-similar solution which can be studied analytically for certain initial velocities. In this case, we consider the initial velocity to be constant and in the normal direction along the curve.

Let the initial curve and velocity be

$$\begin{aligned} \gamma_0(u) &= r_0(\cos u, \sin u), \\ \gamma_1(u) &= -r_1 \vec{N}_0(u) = -r_1(-\cos u, -\sin u) \end{aligned} \tag{10}$$

for $r_0 \in \mathbb{R}_+$, $r_1 \in \mathbb{R}$, $\vec{N}_0$ the inner normal vector of the initial circle. We then obtain the following statement.

Theorem 3.1. *The radially symmetric analytical solution of (7) with the initial condition (10) for $r_1 = 0$ is*

$$r(t) = r_0 \exp\left(-\left(\operatorname{erf}^{-1}\left(t\sqrt{2/r_0^2 \pi} \right) \right)^2 \right), \qquad \text{for } t \in [0,T), \quad T = r_0 \sqrt{\pi/2}.$$

For $r_1 > 0$, the solution is

$$r(t) = r_0 \mathrm{e}^{\frac{r_1^2}{2}} \exp\left(-\left[\operatorname{erf}^{-1}\left(-t\mathrm{e}^{-\frac{r_1^2}{2}} \sqrt{2/r_0^2 \pi} + \operatorname{erf}\left(\frac{r_1}{\sqrt{2}} \right) \right) \right]^2 \right)$$

for $t \in [0, T_s]$, where

$$T_s = \sqrt{\frac{\pi}{2}} r_0 \mathrm{e}^{\frac{r_1^2}{2}} \operatorname{erf}\left(\frac{r_1}{\sqrt{2}}\right).$$

For $t \in [T_s, T)$, the solution is given as the zero velocity solution with the initial radius equal to $r(T_s) = r_0 \mathrm{e}^{\frac{r_1^2}{2}}$.

Proof. Equation (7) for the evolving circle can be rewritten as a second order differential equation for the time-dependent radius $r = r(t)$:

$$\begin{aligned} \ddot{r} &= -\frac{1}{r} \text{ in } (0,T), \\ r(0) &= r_0, \\ \dot{r}(0) &= r_1. \end{aligned} \tag{11}$$

Here, $T > 0$ is defined such that

$$\lim_{t \to T^-} r(t) = 0$$

holds.

Equation (11) is solved analytically. Multiplying it by $\dot{r}$ and integrating over $(0,t)$ for $0 < t < T$, we obtain the identity

$$\dot{r}^2(t) + 2\ln r(t) = r_1^2 + 2\ln r_0, \quad \text{for } t \in [0,T). \tag{12}$$

From (12) we see that $r(t) \le \exp(\frac{1}{2}(r_1^2 + 2\ln r_0))$ and therefore, by (11), there is a constant $C_0 > 0$ such that $r''(t) \le -C_0 < 0$. The solution $r = r(t)$ is then a concave function.

Suppose first that $r_1 \le 0$. Separating the variables in equation (12) and integrating it over $(0,t)$, we obtain the solution implicitly given in the integral form

$$\int_{r_0}^{r(t)} \frac{\mathrm{d}\tilde{r}}{-\sqrt{r_1^2 + 2\ln\frac{r_0}{\tilde{r}}}} = t \tag{13}$$

for $t \in (0,T)$.

Resolving implicit equation (13) for $r_1 = 0$, we find

$$r(t) = r_0 \exp\left(-\left(\operatorname{erf}^{-1}\left(t\sqrt{2/r_0^2\pi}\right)\right)^2\right), \qquad \text{for } t \in [0,T), \quad T = r_0\sqrt{\pi/2}. \tag{14}$$

Here, $\operatorname{erf} : \mathbb{R} \to \mathbb{R}$ is the error function defined as

$$\operatorname{erf}(x) = \frac{2}{\sqrt{\pi}} \int_0^x \mathrm{e}^{-z^2}\,\mathrm{d}z$$

and erf^{-1} is its inverse.

For $r_1 > 0$, the radius first increases until $t = T_s$. Once more, we separate variables in (12) and integrate, this time with the assumption $\dot{r} > 0$ in $(0,T_s)$. Thus, we obtain an implicit solution in $(0,T_s)$ as

$$\int_{r_0}^{r(t)} \frac{\mathrm{d}\tilde{r}}{+\sqrt{r_1^2 + 2\ln\frac{r_0}{\tilde{r}}}} = t. \tag{15}$$

Solving the implicit equation, we obtain solution for $t \in [0,T_s]$ as

$$r(t) = r_0 \mathrm{e}^{\frac{r_1^2}{2}} \exp\left(-\left[\operatorname{erf}^{-1}\left(-t\mathrm{e}^{-\frac{r_1^2}{2}}\sqrt{2/r_0^2\pi} + \operatorname{erf}\left(\frac{r_1}{\sqrt{2}}\right)\right)\right]^2\right) \tag{16}$$

for

$$T_s = \sqrt{\frac{\pi}{2}} r_0 \mathrm{e}^{\frac{r_1^2}{2}} \operatorname{erf}\left(\frac{r_1}{\sqrt{2}}\right).$$

On $[T_s, T)$ the solution continues as the above derived solution for the zero initial velocity (14) with the initial radius equal to

$$r(T_s) = r_0 \mathrm{e}^{\frac{r_1^2}{2}}. \quad \square$$

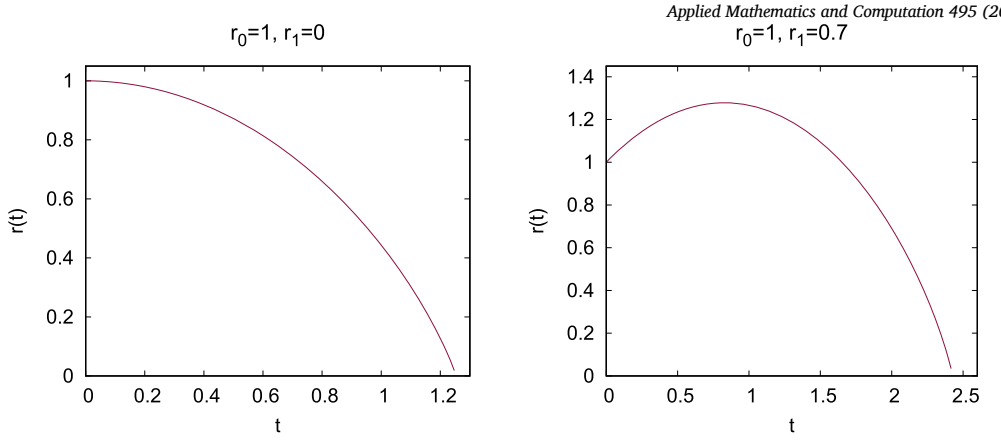

Fig. 1. The analytic solution of equation (11) for $r_0 = 1$, $r_1 = 0$ and for $r_1 = 0.7$ is shown. For the exact form, see (14) and (16).

In Fig. 1, the radius is plotted for the zero as well as non-zero initial velocity.

3.2. Tangential initial velocity

The case of the initial velocity in the tangential direction was not yet studied in the literature. Under specific conditions for the tangential initial velocity we provide an analytic solution of equation (7) for any immersed initial closed curve.

Theorem 3.2. *Let γ_0 be a smooth immersed initial closed curve, and the initial velocity be given as $\gamma_1 = \pm\vec{T}_0$, where $\vec{T}_0 = \frac{1}{|\gamma_0'|}\gamma_0'$. Let $\varphi : S^1 \times [0,T) \to \mathbb{R}$ be a function satisfying the differential equation*

$$\begin{aligned} \partial_t \varphi(u,t) &= \pm \frac{1}{|\gamma_0'(\varphi(u,t))|}, \\ \varphi(u,0) &= u, \end{aligned} \tag{17}$$

for each $u \in S^1$ and $t \in [0,T)$, with the sign given by the sign in the initial velocity.

Then

$$\gamma(u,t) = \gamma_0(\varphi(u,t)), \tag{18}$$

solves equation (7) for the given initial conditions.

Proof. Consider the function given by (18). Then the tangent and the normal vectors are expressed as

$$\begin{aligned} \vec{T}(u,t) &= \frac{\gamma_0'(\varphi(u,t))}{|\gamma_0'(\varphi(u,t))|} \frac{\partial_u \varphi(u,t)}{|\partial_u \varphi(u,t)|}, \\ \vec{N}(u,t) &= \frac{\gamma_0'(\varphi(u,t))^\perp}{|\gamma_0'(\varphi(u,t))|} \frac{\partial_u \varphi(u,t)}{|\partial_u \varphi(u,t)|} \end{aligned}$$

where for a vector $\vec{z} = (z_1, z_2)$, $\vec{z}^\perp$ is defined as $\vec{z}^\perp = (-z_2, z_1)$.

For the existence of the Frenet frame, we need $\partial_u \varphi$ to be either always positive or always negative. The initial condition implies $\varphi(u,0) = u$ which yields $\partial_u \varphi|_{t=0} = 1 > 0$. Thus we suppose $\partial_u \varphi > 0$.

After differentiating γ twice with respect to time

$$\partial_{tt}\gamma(u,t) = \gamma_0''(\varphi(u,t))\partial_t \varphi(u,t)^2 + \gamma_0'(\varphi(u,t))\partial_{tt}\varphi(u,t),$$

the normal acceleration becomes

$$\left\langle \partial_{tt}\gamma(u,t), \vec{N}(u,t) \right\rangle = \frac{\partial_t \varphi(u,t)^2}{|\gamma_0'(\varphi(u,t))|} \left\langle \gamma_0''(\varphi(u,t)), \gamma_0'(\varphi(u,t))^\perp \right\rangle. \tag{19}$$

We want this expression to be equal to curvature. The curvature can be expressed as

$$\kappa(u,t) = \frac{\det(\gamma_0'(\varphi(u,t)), \gamma_0''(\varphi(u,t)))}{|\gamma_0'(\varphi(u,t))|^3}.$$

Notice that

$$\det(\gamma_0'(\varphi(u,t)),\gamma_0''(\varphi(u,t))) = \gamma_{0,1}'(\varphi(u,t))\gamma_{0,2}''(\varphi(u,t)) - \gamma_{0,2}'(\varphi(u,t))\gamma_{0,1}''(\varphi(u,t))$$
$$= \left\langle \gamma_0''(\varphi(u,t)), \gamma_0'(\varphi(u,t))^{\perp} \right\rangle.$$

From there, we deduce that φ must satisfy the equation

$$\partial_t\varphi(u,t)^2 = \frac{1}{|\gamma_0'(\varphi(u,t))|^2},$$

which can be rewritten as

$$\partial_t\varphi(u,t) = \pm\frac{1}{|\gamma_0'(\varphi(u,t))|}. \tag{20}$$

As for the initial condition for φ, we need

$$\gamma(u,0) = \gamma_0(\varphi(u,0)) = \gamma_0(u)$$

which implies

$$\varphi(u,0) = u.$$

The function φ then satisfies the initial-value problem

$$\begin{aligned} &\partial_t\varphi(u,t) = \pm\frac{1}{|\gamma_0'(\varphi(u,t))|} && \text{in } S^1\times(0,+\infty),\\ &\varphi(u,0) = u && \text{in } S^1. \end{aligned} \tag{21}$$

Due to the assumptions, $\gamma(t,u)$ satisfies (21) for $t=0$ and therefore

$$\partial_t\gamma(u,0) = \gamma_0'(u)\partial_t\varphi(u,0) = \pm\vec{T}_0(u).$$

We can see that the initial velocity must be equal to $\pm\vec{T}_0$ to obtain the solution in the form of (18). Moreover, the sign in (20) corresponds to the choice of the sign of the initial velocity in the assumptions of Theorem 3.2.

We calculate the tangential acceleration

$$\left\langle \partial_{tt}\gamma(\varphi(u,t)), \vec{T}(u,t)\right\rangle = \frac{\partial_t\varphi(u,t)^2}{|\gamma_0'(\varphi(u,t))|}\left\langle \gamma_0''(\varphi(u,t)), \gamma_0'(\varphi(u,t))\right\rangle + |\gamma_0'(\varphi(u,t))|\partial_{tt}\varphi(u,t). \tag{22}$$

From (21), we evaluate $\partial_{tt}\varphi$:

$$\partial_{tt}\varphi(u,t) = \pm\partial_t\left(\frac{1}{|\gamma_0'(\varphi(u,t))|}\right) = -\frac{\langle\gamma_0'(\varphi(u,t)),\gamma_0''(\varphi(u,t))\rangle}{|\gamma_0'(\varphi(u,t))|^4}.$$

When substituting $\partial_t\varphi$ and $\partial_{tt}\varphi$ back into expression (22), we observe that the tangential acceleration is zero:

$$\langle\partial_{tt}\gamma(u,t),\vec{T}(u,t)\rangle = \frac{\langle\gamma_0'(\varphi(u,t)),\gamma_0''(\varphi(u,t))\rangle}{|\gamma_0'(\varphi(u,t))|^3} - \frac{\langle\gamma_0'(\varphi(u,t)),\gamma_0''(\varphi(u,t))\rangle}{|\gamma_0'(\varphi(u,t))|^3} = 0.$$

On the right-hand side of (7), the prescribed tangential acceleration becomes

$$\begin{aligned} &-\frac{1}{|\gamma_0'(\varphi(u,t))|}\langle\partial_{ut}\gamma(\varphi(u,t)),\partial_t\gamma(\varphi(u,t))\rangle\\ &= -\frac{1}{|\gamma_0'(\varphi(u,t))|}\left\langle\partial_u(\gamma_0'(\varphi(u,t))\partial_t\varphi(u,t),\gamma_0'(\varphi(u,t))\partial_t\varphi(u,t)\right\rangle\\ &= -\left\langle\frac{1}{|\gamma_0'(\varphi(u,t))|}\partial_u\left(\pm\frac{\gamma_0'(\varphi(u,t))}{|\gamma_0'(\varphi(u,t))|}\right),\pm\frac{\gamma_0'(\varphi(u,t))}{|\gamma_0'(\varphi(u,t))|}\right\rangle\\ &= -\left\langle\frac{1}{|\gamma_0'(\varphi(u,t))|}\partial_u\vec{T}_0(u,t),\vec{T}_0(u,t)\right\rangle \end{aligned}$$

and from the Frenet formulae, we obtain

$$-\left\langle\frac{1}{|\gamma_0'(\varphi(u,t))|}\partial_u\vec{T}_0(\varphi(u,t)),\vec{T}_0(\varphi(u,t))\right\rangle = -\left\langle\kappa_0(\varphi(u,t))\vec{N}_0(\varphi(u,t)),\vec{T}_0(\varphi(u,t))\right\rangle = 0.$$

Therefore, the curve γ is a solution of equation (7). □

Example. To illustrate Theorem 3.2, we set the initial curve as a circle with the radius r_0. Then equation (17) can be rewritten as $\partial_t\varphi = \pm\frac{1}{r_0}, \varphi(u,0) = u$. The right-hand side is constant, therefore its solution is $\varphi(u,t) = \pm\frac{1}{r_0}t + u$ and the form of γ is

$$\gamma(u,t) = r_0\left(\cos(\pm\tfrac{1}{r_0}t + u), \sin(\pm\tfrac{1}{r_0}t + u)\right). \tag{23}$$

The sign in $\pm$ corresponds to the choice of the sign in the initial velocity in Theorem 3.2.

Consequence. Note, that any immersed initial curve can be arc-length reparametrized. For such an initial curve, equation (17) is reduced to equation $\partial_t\varphi = \pm 1, \varphi(u,0) = u$ with the solution $\varphi(u,t) = \pm t + u$. This proves that the solution of (17) can always be found for any immersed initial curve.

4. Numerical scheme

In the previous part of the text, we presented several analytically solvable cases. Below, we derive a numerical scheme which will approximate the solution of (7) and its modification (9) in a more general setup of the initial conditions. For this purpose, we describe the discretization of evolution law (7) and its modification (9) by means of the finite-volume/finite-difference method. In [12], a fully discrete finite-difference scheme with constant time step using three consecutive time levels is proposed. In our case, we discretize (7), (9) in the parameter space to design semi-discrete schemes as systems of ODE's, which are then solved by more accurate higher-order time solvers of Runge-Kutta type with adaptive time step. Additionally, we design an original redistribution procedure based on (9) which further stabilizes the algorithm.

The evolving closed curve $\gamma(u,t)$ defined on $[0,2\pi]\times[0,T)$ is approximated by a piecewise linear curve (polygon) given by the set of discrete points $\gamma^j(t) = \gamma(j\frac{2\pi}{N}, t)$ for $j \in \{1,2,\dots,N\}$ where N is the number of discretization points. Notice that for a closed curve the periodic boundary conditions hold, i.e. $\gamma^0 = \gamma^N$ and $\gamma^{N+1} = \gamma^1$. In the following approximations and schemes we denote

$$h = \frac{2\pi}{N},\ d_c^j = |\gamma^{j+1} - \gamma^{j-1}| \text{ and } d^j = |\gamma^{j+1} - \gamma^j|. \tag{24}$$

Using finite differences we approximate the term $\kappa\vec{N}$ at $u = jh$ (denoted by upper index j):

$$\left[\frac{1}{|\partial_u\gamma|}\partial_u\left(\frac{\partial_u\gamma}{|\partial_u\gamma|}\right)\right]^j \approx \frac{2}{d_c^j}\left(\frac{\gamma^{j+1}-\gamma^j}{d^j} - \frac{\gamma^j - \gamma^{j-1}}{d^{j-1}}\right). \tag{25}$$

This approximation is of second order.

By the same order, we approximate $\langle\partial_{st}\gamma, \partial_t\gamma\rangle$ as

$$\left[\left\langle\frac{\partial_{ut}\gamma}{|\partial_u\gamma|}, \partial_t\gamma\right\rangle\right]^j \approx \frac{1}{d_c^j}\langle\dot\gamma^{j+1} - \dot\gamma^{j-1}, \dot\gamma^j\rangle, \tag{26}$$

where $\dot\gamma^j = \partial_t\gamma(jh,t)$.

Discrete Evolution Law 1. Equation (7) is approximated by the **semi-discrete scheme** which is a system of $2N$ *second-order* ordinary differential equations

$$\begin{aligned}
\ddot\gamma^j =& \frac{2}{d_c^j}\left(\frac{\gamma^{j+1}-\gamma^j}{d^j} - \frac{\gamma^j-\gamma^{j-1}}{d^{j-1}}\right) - \langle\dot\gamma^{j+1} - \dot\gamma^{j-1}, \dot\gamma^j\rangle\frac{(\gamma^{j+1}-\gamma^{j-1})}{(d_c^j)^2}, \quad j = 1,\dots,N\\
\gamma^0 =& \gamma^N, \quad \gamma^{N+1} = \gamma^1,\\
\gamma^j(0) =& \gamma_0(jh),\\
\dot\gamma^j(0) =& \gamma_1(jh), \quad j = 1,\dots,N.
\end{aligned} \tag{27}$$

To discretize modified evolution law (9), we approximate $\tilde\alpha$ as

$$\left[\frac{1}{|\partial_u\gamma|^3}\langle\partial_{uu}\gamma, \partial_u\gamma\rangle\right]^j \approx \frac{4}{(d_c^j)^3}\left\langle\left(\gamma^{j-1} - 2\gamma^j + \gamma^{j+1}\right), \left(\gamma^{j+1} - \gamma^{j-1}\right)\right\rangle.$$

The tangent vector of the four-dimensional curve $(\gamma,\eta)^\top$ is approximated as

$$\left[\vec{\tilde T}\right]^j = \left[\frac{1}{\sqrt{|\partial_u\gamma|^2 + |\partial_u\eta|^2}}\begin{pmatrix}\partial_u\gamma\\ \partial_u\eta\end{pmatrix}\right]^j \approx \frac{1}{\tilde d_c^j}\begin{pmatrix}\gamma^{j+1}-\gamma^{j-1}\\ \eta^{j+1}-\eta^{j-1}\end{pmatrix},$$

for

$$\tilde d_c^j = \sqrt{|\gamma^{j+1}-\gamma^{j-1}|^2 + |\eta^{j+1}-\eta^{j-1}|^2}.$$

Those approximations are of second-order as well.

Discrete Evolution Law 2. Equation (9) is approximated by the **semi-discrete scheme** which is a system of $4N$ *first-order* ordinary differential equations:

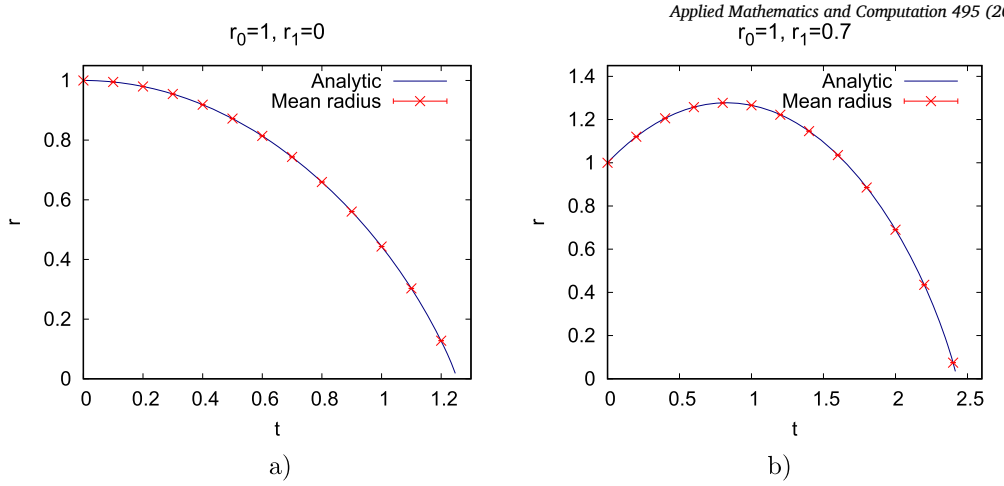

Fig. 2. The comparison between the mean radius $\overline{r}$ of the numerically computed evolving circle (red crosses) and the analytic solution (blue line); example with the zero initial velocity on the left, and example with the non-zero normal initial velocity on the right. The mean radius is computed with the time step 0.1 on the left and with the time step 0.2 on the right. Number of mesh points was $N = 300$ in both cases.

$$
\begin{aligned}
\dot{\gamma}^j =& \eta^j + \frac{4}{\tilde{d}_c^j (d_c^j)^3} \left\langle \left(\gamma^{j-1} - 2\gamma^j + \gamma^{j+1}\right), \left(\gamma^{j+1} - \gamma^{j-1}\right) \right\rangle \left(\gamma^{j+1} - \gamma^{j-1}\right), \\
\dot{\eta}^j =& \frac{2}{d_c^j} \left(\frac{\gamma^{j+1} - \gamma^j}{d^j} - \frac{\gamma^j - \gamma^{j-1}}{d^{j-1}} \right) - \langle \eta^{j+1} - \eta^{j-1}, \eta^j \rangle \frac{(\gamma^{j+1} - \gamma^{j-1})}{(d_c^j)^2} \\
&+ \frac{4}{\tilde{d}_c^j (d_c^j)^3} \left\langle \left(\gamma^{j-1} - 2\gamma^j + \gamma^{j+1}\right), \left(\gamma^{j+1} - \gamma^{j-1}\right) \right\rangle \left(\eta^{j+1} - \eta^{j-1}\right), \quad j = 1, \dots, N \\
\gamma^0 =& \gamma^N, \quad \gamma^{N+1} = \gamma^1, \quad \eta^0 = \eta^N, \quad \eta^{N+1} = \eta^1, \\
\gamma^j(0) =& \gamma_0(jh), \\
\eta^j(0) =& \gamma_1(jh), \quad j = 1, \dots, N.
\end{aligned}
\tag{28}
$$

Scheme (27) approximates evolution law (7), and scheme (28) approximates evolution law (9) with the order of approximation $\mathcal{O}(h^2)$ in space as follows from this behavior for each particular term of the right-hand sides mentioned above. Both schemes as the systems of ordinary differential equations in variables $\gamma_1(t), \dots, \gamma_N(t)$ can be understood as autonomous with locally Lipschitz-continuous right-hand sides, and in the initial-value problem are locally solvable due to the Picard theorem, see [39]. Global solvability as well as convergence of their solutions to the solutions of problems (27) and (7) are beyond the scope of this text.

In the subsequent computations, both systems of ordinary differential equations (27) and (28) are numerically solved using the Runge-Kutta-Merson method with adaptive time step as in [36,43,7]. The time-step adaptivity tolerance was set to 10^{-6} in all computations.

5. Computational examples

Schemes (27) and (28) were used to obtain a numerical solution of evolution laws (7) and (9). In this section, the numerical solution is compared with the analytic one and the computational examples for various initial conditions are presented.

5.1. Quantitative computations

As derived in Section 3, the analytical solution of (7) exists and has the form of an evolving circle. It can be used to verify behavior of numerical scheme (27) by comparison with it (similarly to [12] - Tab. 1). For this purpose, we prescribe the initial condition as in (10) and evaluate it on a uniform mesh along the interval $[0, 2\pi]$ as in (24). We recall that there is no guaranty that the line segments d_c^j and d^j are kept of uniform magnitude during the curve evolution. This fact motivates the improvement in the form of the problem (9) discussed below.

For a given numerical solution of (27) of the radially symmetric problem represented by N points $(\gamma^j)_{j=1}^N$, we define the mean radius as $\overline{r} = \left(\sum_{j=1}^N |\gamma^j| \right) / N$.

To measure the deviation from the value of $\overline{r}$, the standard deviation σ is given as a square root from $\sigma^2 = \left(\sum_{j=1}^N (|\gamma^j| - \overline{r})^2 \right) / N$.

The comparison between the mean radius of the numerically computed evolving circle and its analytic value is presented in Fig. 2, considering the example with the zero initial velocity as well as the example with the non-zero normal velocity. The numerical solution was computed using $N = 300$ points. The values of the absolute error and σ are presented in Table 1.

Table 1
The left table corresponds to Fig. 2 a), and the right table corresponds to Fig. 2 b). In the second column of the tables, the evaluated absolute difference between the mean radius of the numerical solution $\bar{r}$ and the analytical value $r(t)$ is presented for given time levels. In the third column, the values of standard deviation σ are shown.

$r_1 = 0$		
t	$\lvert\bar{r} - r(t)\rvert$	σ
0	0	3.09×10^{-17}
0.1	1.76×10^{-7}	6.41×10^{-15}
0.2	7.03×10^{-7}	6.28×10^{-13}
0.3	2.20×10^{-6}	3.21×10^{-11}
0.4	4.31×10^{-6}	1.44×10^{-9}
0.5	7.30×10^{-6}	1.53×10^{-9}
0.6	1.09×10^{-5}	2.53×10^{-10}
0.7	1.44×10^{-5}	4.68×10^{-10}
0.8	2.04×10^{-5}	9.64×10^{-11}
0.9	2.68×10^{-5}	3.86×10^{-9}
1	3.49×10^{-5}	3.97×10^{-9}
1.1	4.62×10^{-5}	4.06×10^{-10}
1.2	6.64×10^{-5}	5.90×10^{-11}

a)

$r_1 = 0.7$		
t	$\lvert\bar{r} - r(t)\rvert$	σ
0	0	3.09×10^{-17}
0.2	2.78×10^{-6}	3.29×10^{-13}
0.4	2.22×10^{-7}	8.83×10^{-10}
0.6	4.78×10^{-6}	5.77×10^{-10}
0.8	1.92×10^{-5}	3.30×10^{-10}
1	2.44×10^{-5}	8.58×10^{-11}
1.2	4.05×10^{-5}	1.63×10^{-9}
1.4	5.27×10^{-5}	9.70×10^{-10}
1.6	6.99×10^{-5}	6.42×10^{-9}
1.8	9.12×10^{-5}	2.33×10^{-10}
2	1.21×10^{-4}	1.72×10^{-9}
2.2	1.67×10^{-4}	7.06×10^{-10}
2.4	2.81×10^{-4}	2.59×10^{-10}

b)

Table 2
The experimental order of convergence for evolving unit circle for zero and non-zero initial normal velocity r_1. Parameters for the computation were $m = 12$ for both cases, $\hat{\tau} = 0.1$ on the left and $\hat{\tau} = 0.2$ on the right. The exact solution was represented by a polygonal curve with 1600 vertices in both cases.

$r_1 = 0$		
N_i	$\lVert e^{(i)}\rVert_w$	EOC(N_{i-1}, N_i)
50	0.002085	–
100	0.000522	1.999
200	0.000131	1.995
400	0.000033	1.974
800	0.000009	1.894

$r_1 = 0.7$		
N_i	$\lVert e^{(i)}\rVert_w$	EOC(N_{i-1}, N_i)
50	0.004866	–
100	0.001215	2.002
200	0.000306	1.991
400	0.000079	1.952
800	0.000023	1.809

The rate of convergence of the numerical solution to the analytic solution with the increasing number of grid points N, called the experimental order of convergence (EOC) can be evaluated as in, e.g. [13], or in [3,4].

The EOC is calculated in the following way. Let N_i be $i-$th element of an increasing sequence of number of grid points. Let $\hat{\gamma}(\cdot, t)$ be a very fine piece-wise linear (polygonal) approximation of the exact solution of problem (7) - in the presented computations, it uses 1600 vertices. Let $\gamma_i(\cdot, t)$ be piecewise-linear (polygonal) representation of the numerical solution obtained by scheme (27) with N_i discretization points. We then denote by $e_k^{(i)}$ the Hausdorff distances between the exact solution $\hat{\gamma}$ and curve γ^i at the times $k\hat{\tau}$, where $\hat{\tau}$ is the given time step between the measurements and $k = 0, 1, 2, \ldots, m$ for m a given number of measurements.

Remark. The Hausdorff distances between the polygonal curves considered above are evaluated (and, in fact, approximated) by collecting distances of a segment of one curve from all segments of other curve. Mutual distances between segments are obtained approximatively by considering distances of a larger number of individual points of one segment from other segment and vice versa.

Then we calculate the weighted L^2 norm of Hausdorff distances over the time levels as

$$\|e^{(i)}\|_w = \left(\frac{1}{m+1} \sum_{k=0}^{m} (e_k^{(i)})^2 \right)^{1/2}.$$

The experimental order of convergence is obtained for two consecutive grids with N_{i-1} and N_i mesh points as

$$EOC(N_{i-1}, N_i) = \frac{\log(\|e^{(i-1)}\|_w / \|e^{(i)}\|_w)}{\log(N_i / N_{i-1})}.$$

In Table 2, the convergence analysis is presented for the evolving circle. The exact solution was represented by a piece-wise linear curve (polygon) with 1600 vertices in both cases. The calculated EOCs are close to the value of two. This is in accordance with scheme (27) which is of the second-order accuracy in space.

Next we investigate convergence of the numerical solution obtained by scheme (28) for a nonuniformly divided initial condition (10) as

$$\begin{aligned} \gamma_0(jh) &= r_0(\cos\phi(jh), \sin\phi(jh)), \\ \gamma_1(jh) &= r_1(\cos\phi(jh), \sin\phi(jh)) \end{aligned} \tag{29}$$

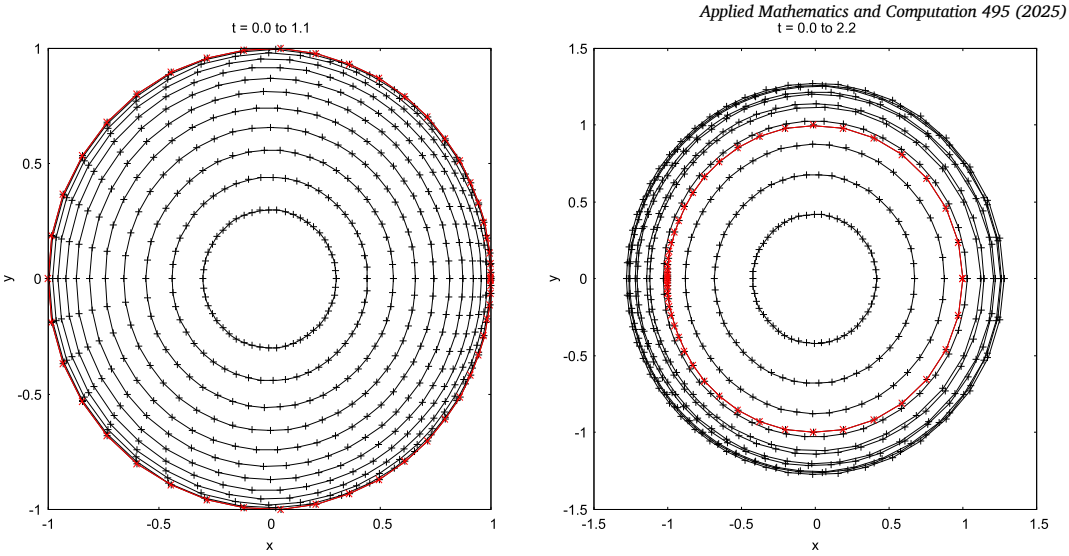

Fig. 3. On the left, the evolution of the initially non-uniformly discretized circle ($\phi(u) = 2\pi(3(u/2\pi)^2 - 2(u/2\pi)^3)$) with the zero initial velocity. The time step between the presented time levels is 0.1, number of points is $N = 50$. On the right, the evolution of the initially non-uniformly discretized circle ($\phi(u) = u + \frac{10}{11}\sin u$) with the initial velocity $r_1 = 0.7$. The time step between the presented time levels is 0.2, number of points is $N = 50$.

Table 3
The experimental order of convergence for the evolving unit circle with the initially non-uniform discretization for zero and non-zero initial normal velocity r_1. Parameters for the computation were $m = 11$ for both cases, $\hat{\tau} = 0.1$ on the left and $\hat{\tau} = 0.2$ on the right. The exact solution was represented by a polygonal curve with 1600 vertices in both cases.

$r_1 = 0$		
N_i	$\|e^{(i)}\|_w$	EOC(N_{i-1}, N_i)
50	0.004219	–
100	0.001057	1.997
200	0.000267	1.985
400	0.000072	1.901
800	0.000021	1.743

$r_1 = 0.7$		
N_i	$\|e^{(i)}\|_w$	EOC(N_{i-1}, N_i)
50	0.0215070	–
100	0.0053893	1.997
200	0.0013500	1.997
400	0.0003403	1.988
800	0.0000884	1.944

where $\phi(u) = 2\pi(3(u/2\pi)^2 - 2(u/2\pi)^3)$, resp. $\phi(u) = u + \frac{a}{1+a}\sin u$ with $a = 10$, $r_0 = 1.0$ and $r_1 = 0.0$ or $r_1 = 0.7$, $u \in [0, 2\pi]$. The curve dynamics is shown in Fig. 3. In Table 3, the convergence analysis is presented for this case indicating values similar to Table 2.

5.2. Qualitative computations

Once the numerical algorithm is verified, we demonstrate a selection of patterns developed during the evolution by the motion law (7) with the zero initial velocity solved by scheme (27) using a suitable number of discretization points justified by experience from quantitative computations. During the evolution we observe interesting behavior which can be explained as the onset of singularities predicted by theory. Computations stop before the singularities develop. The results are depicted in Figs. 4, 5, 6 and 7.

Convexity preservation is studied in Fig. 4, where the evolution of two initially convex curves is illustrated. On the left, the initial curve is in the form of the unit ball in the L^3-norm ($|x|^3 + |y|^3 = 1$). It shrinks while its shape vibrates between two patterns whose corners seem to sharpen. On the right, the initial ellipse with the length of semi-axes equal to 1.5 and 1 shrinks and tends to a vertically oriented pattern with narrowing the upper and lower parts (compare with [12], Fig. 2). Both curves stay convex during the computation. This observation illustrates the convexity preservation, which was proved in [29]. The computation stops before any singularity predicted by Theorem 1.2 in [29] occurs.

Containment (comparison) principle is illustrated in Fig. 5. We can see the evolution the initial curve in the form of the unit ball in the L^3-norm as above inside of its circumscribed circle. As expected, both curves never cross each other.

Evolution of non-convex patterns is shown in Figs. 6 and 7. The first case starts with a 3-folded curve whose shape oscillates between two shrinking 3-folded forms with variable sign of curvature. Apparently the petals tend to sharpen. The second case starts with the Cassini curve (compare with similar curve in [12], Fig. 6) which converts to an elongated shape and then becomes non-convex from the sides and again tends to develop corners as predicted by the mentioned theory. Both computations stop before the singularity appears. At the time close to it, the numerical scheme is not stable.

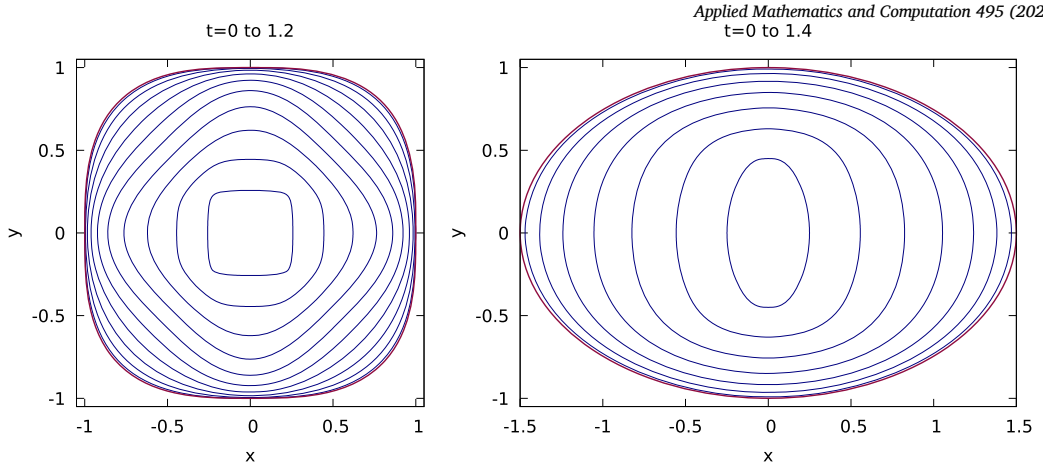

Fig. 4. Evolution of two convex curves under HCSF equation (7) with zero initial velocity. The time step between the presented time levels is 0.12, number of points is $N = 500$.

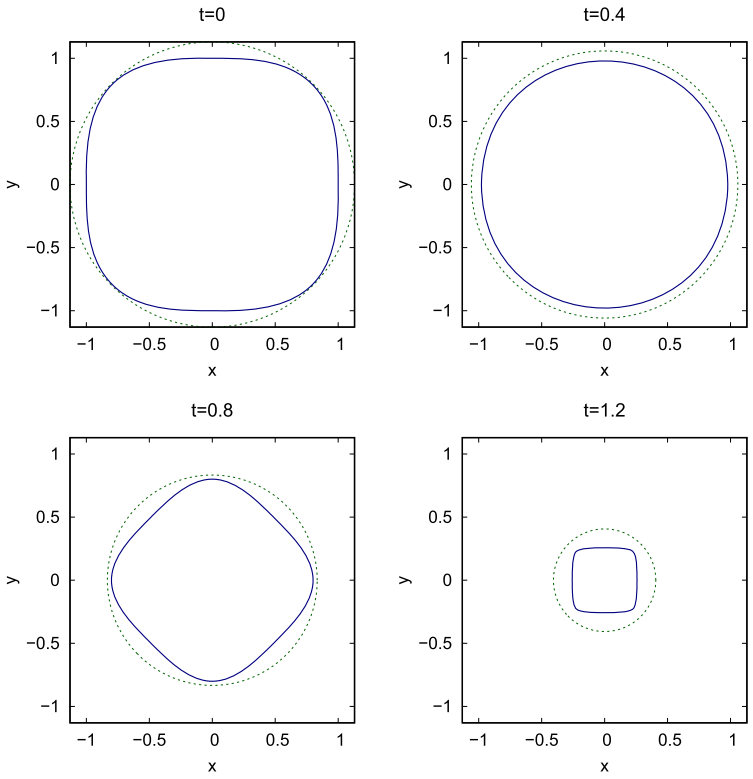

Fig. 5. Evolving convex curve from Fig. 4 inside an evolving circle, both with zero initial velocity - the containment principle is illustrated.

Effect of non-zero initial tangential velocity is studied in Figs. 8 and 9. The motion law (7) solved by scheme (27) is influenced by the choice of the tangential velocity $\gamma_1 = c\vec{T}_0$, $c \in \mathbb{R}$. In Fig. 8, the evolution of the unit circle is presented for various values of c. As follows from Theorem 3.2, the curve will not change its shape during the evolution for $c = \pm 1$. This was verified numerically in Fig. 8. For $|c| < 1$, the circle shrinks to the point slower than for the zero initial velocity. For $|c| > 1$, we observe that the circle starts to grow. This behavior resembles the effect of the centrifugal force. In Fig. 9, the effect of the tangential initial velocity with $c = 0.2$ on evolution of the ellipse is presented. We can see the deformation of the evolving curve and the prolongation of the evolution.

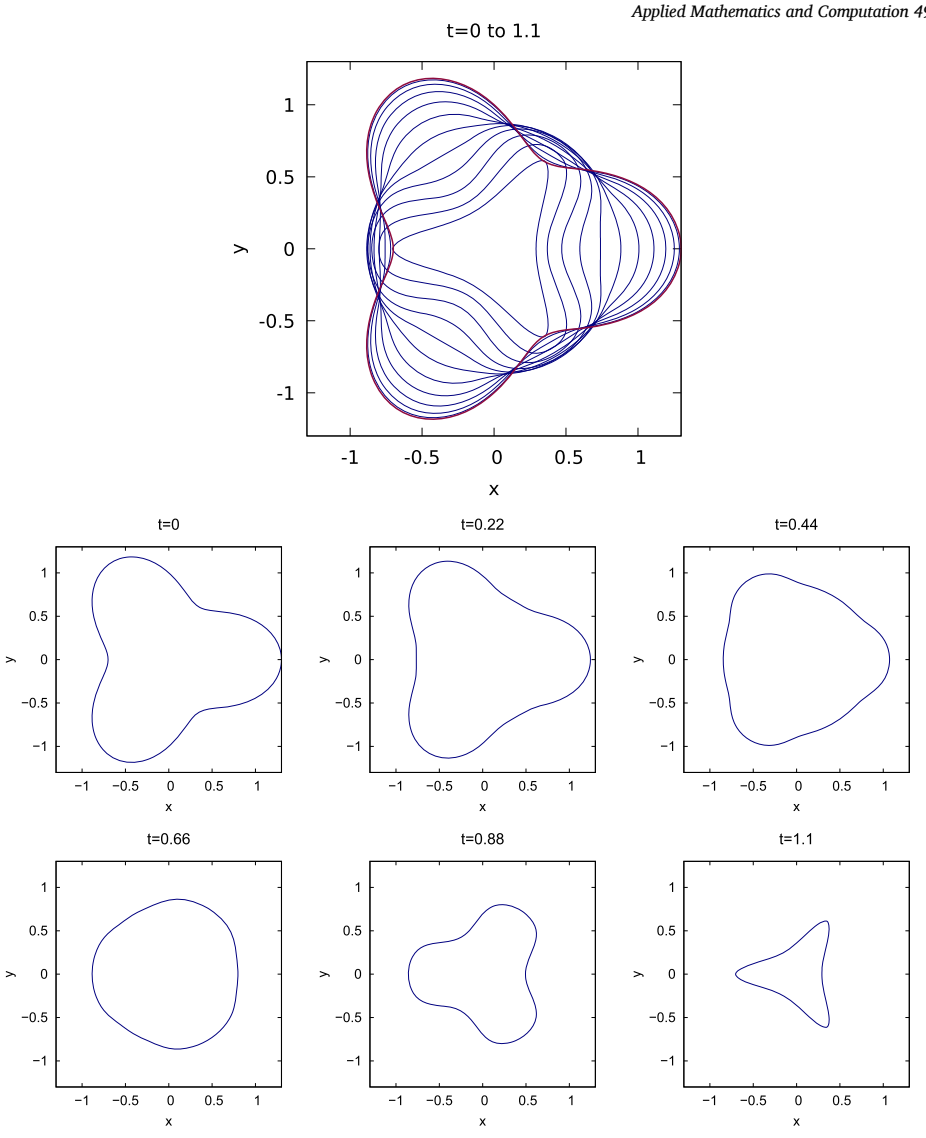

Fig. 6. Evolving non-convex curve with zero initial velocity. In the top picture, the time step between the presented time levels is 0.1. Number of points is $N = 400$.

5.3. Redistribution

Uniform distribution of the discretization points during the curve evolution contributes to the stability of numerical schemes for the curve dynamics. The evolution law (9) was derived for this purpose. In Fig. 10, the evolution of the Cassini curve

$$\gamma_0(u) = p\sqrt{\cos 2u + \sqrt{\left(\frac{q}{p}\right)^4 - \sin^2 2u}}\,(\cos u, \sin u),\ p = 0.95,\ q = 1$$

by equation (7) solved by (27) is compared with the evolution according to equation (9) solved by (28), both with the zero initial velocity. The evolution example confirms that the shape of the evolving curve is not changed. However the discretization points generated by (28) are distributed uniformly during the evolution.

In Fig. 11, the evolution of the Cassini initial curve ($p = 0.99$, $q = 1$) by (28) is presented. For this case, a convergence study is presented where the numerical solution in the form of a polygonal curve for $N = 50, 100, 200, 400, 800$ is compared with the very fine solution in the form of a polygonal curve for $N = 1600$ by means of the Hausdorff distance - see Table 4.

In Fig. 12, the evolution of a 5-folded initial curve by (28) is presented with a typical pattern alternation. For this case, a convergence study is presented where the numerical solution in the form of a polygonal curve for $N = 50, 100, 200, 400, 800$ is compared with the very fine solution in the form of a polygonal curve for $N = 1600$ by means of the Hausdorff distance - see Table 5.

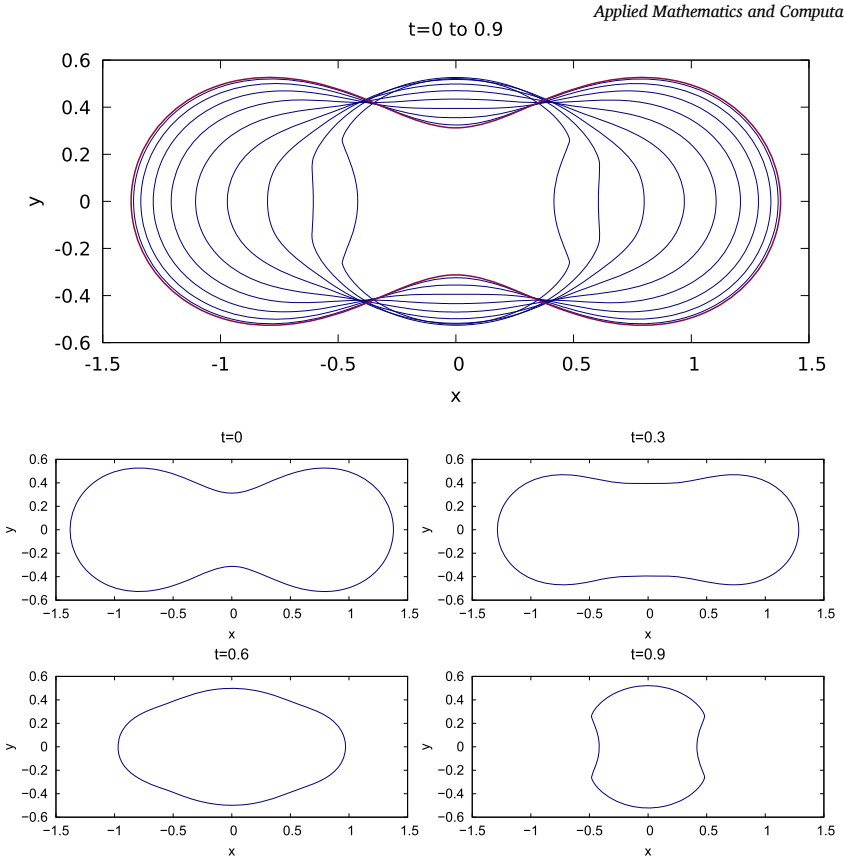

Fig. 7. The evolution of the Cassini curve with zero initial velocity under equation (7). In the top picture, the time step between the presented time levels is 0.1. Number of points is $N = 400$.

Table 4
The experimental order of convergence for the Cassini curve is evaluated. The very fine solution was obtained using $N = 1600$.

Cassini curve		
N_i	$\|e^{(i)}\|_w$	EOC(N_{i-1}, N_i)
50	0.0132919	–
100	0.0045971	1.532
200	0.0016012	1.522
400	0.0004968	1.688
800	0.0001141	2.122

Table 5
The experimental order of convergence for the 5-folded curve is evaluated. The very fine solution was obtained using $N = 1600$.

5-folded curve		
N_i	$\|e^{(i)}\|_w$	EOC(N_{i-1}, N_i)
50	0.0137570	–
100	0.0040137	1.777
200	0.0012216	1.716
400	0.0003050	2.002
800	0.0000619	2.300

6. Conclusion

Computational studies by a semi-discrete finite-volume scheme supported by a class of existing analytical solutions allowed to study behavior of the solution representing convex as well as non-convex curves. The scheme was stabilized by a redistribution method derived in a specific way. Future investigation will be focused on the curve evolution influenced by external forces.

Acknowledgement

The authors are grateful for discussion and comments by Prof. Daniel Ševčovič, Comenius University in Bratislava. This work was partly supported by The Ministry of Education, Youth and Sports of the Czech Republic under the OP RDE Grant No. *CZ.02.1.01/0.0/0.0/16019/0000778*, by the project *21-09093S* of the Czech Science Foundation, and by the CTU under the grant No. *SGS23/188/OHK4/3T/14*.

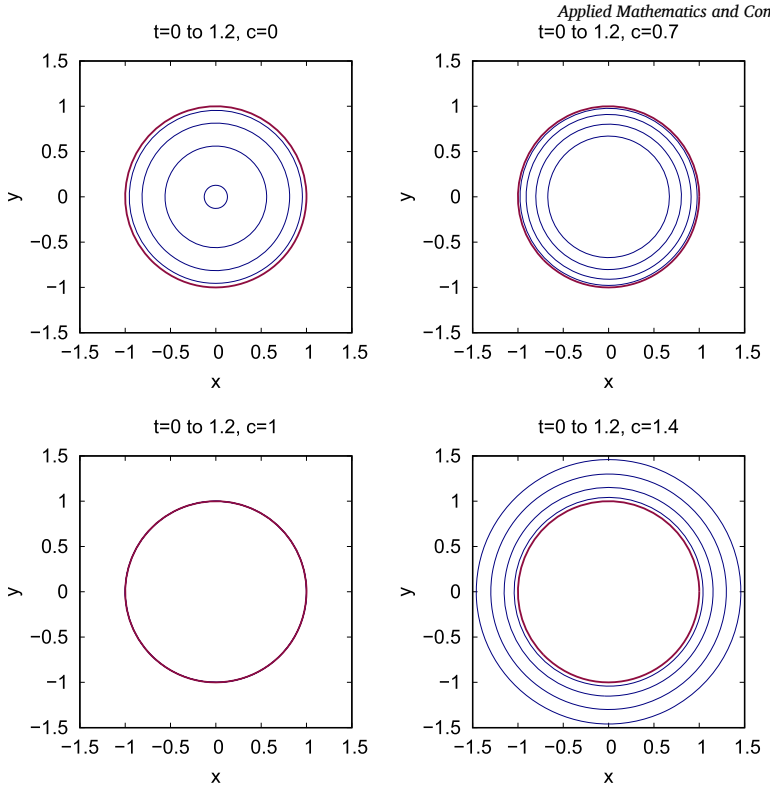

Fig. 8. Evolution of circle for various initial tangential velocities; $\gamma_1 = c\vec{T}_0$ for various values of c. The time step between the depicted time levels is 0.3. The red circle represents the initial curve. Number of points is $N = 400$.

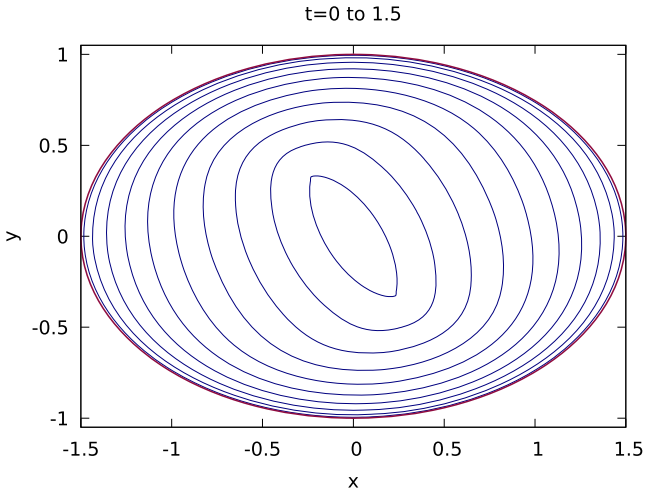

Fig. 9. Evolving ellipse with the initial tangential velocity $\gamma_1 = 0.2\vec{T}_0$. The time step between the depicted time levels is 0.15. Number of points is $N = 500$.

Data availability

No data was used for the research described in the article.

References

[1] S.J. Altschuler, M.A. Grayson, Shortening space curves and flow through singularities, J. Differ. Geom. 35 (1992) 283–298.
[2] A.F. Andreev, A.Y. Parshin, Equilibrium shape and oscillations of the surface of quantum crystals, Sov. Phys. JETP 48 (4) (1978) 763–766.
[3] M. Beneš, Diffuse-interface treatment of the anisotropic mean-curvature flow, Appl. Math. 48 (6) (2003) 437–453.

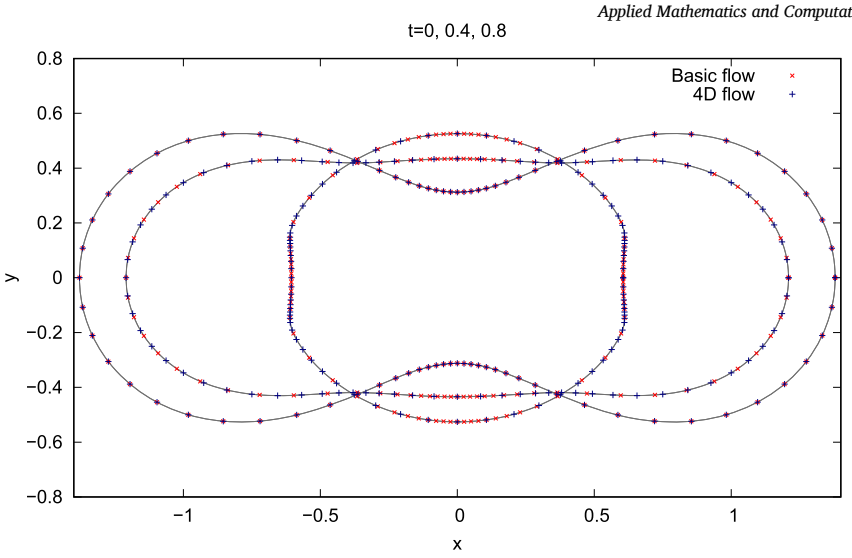

Fig. 10. The comparison between the evolution of the Cassini curve using flow (7) (red crosses) and flow (9) (blue plus sign). The shape of evolving curve did not change with the 4D modification while the distribution of the points changed significantly in the beginning of the evolution. Number of discretization points is $N = 400$ and only every fifth point is plotted for better clarity.

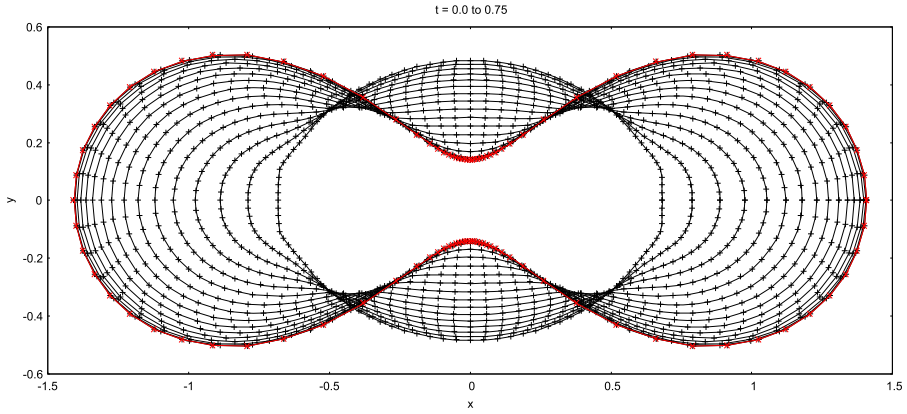

Fig. 11. The evolution of the Cassini curve using (9) with the effect of redistribution on $N = 100$.

[4] M. Beneš, Computational studies of anisotropic diffuse interface model of microstructure formation in solidification, Acta Math. Univ. Comen. 76 (1) (2007) 39–50.
[5] M. Beneš, J. Kratochvíl, J. Křišťan, V. Minárik, P. Pauš, A parametric simulation method for discrete dislocation dynamics, Eur. Phys. J. Spec. Top. 177 (1) (2009) 171–191.
[6] M. Beneš, M. Kolář, D. Ševčovič, Qualitative and numerical aspects of a motion of a family of interacting curves in space, SIAM J. Appl. Math. 82 (2) (2022) 549–575.
[7] M. Beneš, D. Ševčovič, M. Kolář, Curvature driven flow of a family of interacting curves with applications, Math. Methods Appl. Sci. 43 (2020) 4177–4190.
[8] Q. Cheng, C.-L. He, S.-J. Huang, Remarks on the normal hyperbolic mean curvature flow, Anal. Appl. 22 (02) (2024) 407–423.
[9] K.-S. Chou, W. Wo, On hyperbolic Gauss curvature flows, J. Differ. Geom. 89 (3) (2011) 455–485.
[10] K. Deckelnick, Weak solutions of the curve shortening flow, Calc. Var. Partial Differ. Equ. 5 (6) (1997) 489–510.
[11] K. Deckelnick, G. Dziuk, L. Ambrosio, M. Mimura, V. Solonnikov, H.M. Soner, Numerical Approximation of Mean Curvature Flow of Graphs and Level Sets, Springer-Verlag, Berlin Heidelberg, July 2004, pp. 295–446.
[12] K. Deckelnick, R. Nürnberg, Discrete hyperbolic curvature flow in the plane, SIAM J. Numer. Anal. 61 (4) (2023) 1835–1857.
[13] G. Dziuk, Convergence of a semi-discrete scheme for the curve shortening flow, Math. Models Methods Appl. Sci. 4 (4) (1994) 589–606.
[14] G. Dziuk, K. Deckelnick, C.M. Elliott, Computation of geometric partial differential equations and mean curvature flow, Acta Numer. 14 (2005) 139–232.
[15] M. Gage, Curve shortening makes convex curves circular, Invent. Math. 76 (1984) 357–364.
[16] M. Gage, R.S. Hamilton, The heat equation shrinking convex plane curves, J. Differ. Geom. 23 (1986) 69–96.
[17] B. Gao, Q. lian Yin, Symmetries and conservation laws associated with a hyperbolic mean curvature flow, Appl. Math. J. Chin. Univ. 37 (2022) 583–597.
[18] B. Gao, L. Yang, Symmetries of the one-dimensional hyperbolic Lagrangian mean curvature flow, Pramana J. Phys. 97 (2023) 104.
[19] E. Ginder, K. Švadlenka, Wave-type threshold dynamics and the hyperbolic mean curvature flow, Jpn. J. Ind. Appl. Math. 33 (2016) 501–523.
[20] M. Gurtin, A mechanical theory for crystallization of a rigid solid in a liquid melt; melting-freezing waves, Arch. Ration. Mech. Anal. 110 (1990) 287–312.
[21] M.E. Gurtin, P. Podio-Guidugli, A hyperbolic theory for the evolution of plane curves, SIAM J. Math. Anal. 22 (3) (1991) 575–586.
[22] C. He, S. Huang, X. Xing, Self-similar solutions to the hyperbolic mean curvature flow, Acta Math. Sci. 37 (3) (2017) 657–667.
[23] C.-L. He, D.-X. Kong, K. Liu, Hyperbolic mean curvature flow, J. Differ. Equ. 246 (1) (2009) 373–390.

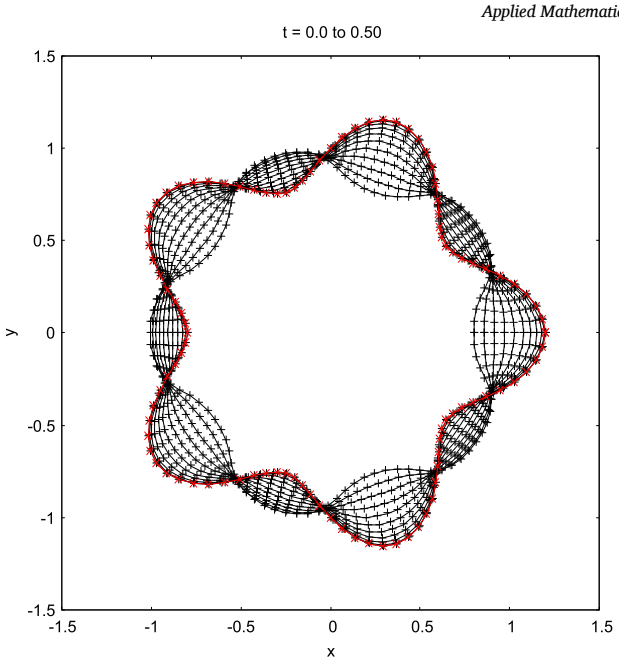

Fig. 12. The evolution of the 5-folded curve using (9) with the effect of redistribution on $N = 100$.

[24] S. Ishida, M. Yamamoto, R. Ando, T. Hachisuka, A hyperbolic geometric flow for evolving films and foams, ACM Trans. Graph. 36 (6) (2017) 199:1–199:11.
[25] M. Kang, A level set approach for the motion of soap bubbles with curvature dependent velocity or acceleration, PhD thesis, University of California, Los Angeles, 1996.
[26] M. Kang, B. Merriman, S. Osher, Numerical simulations for the motion of soap bubbles using level set methods, Comput. Fluids 37 (5) (2008) 524–535.
[27] K.O. Keshishev, A.Y. Parshin, A.V. Babkin, Experimental detection of crystallization waves in He^4, JETP Lett. 30 (1979) 56–59.
[28] M. Kolář, P. Pauš, J. Kratochvíl, M. Beneš, Improving method for deterministic treatment of double cross-slip in FCC metals under low homologous temperatures, Comput. Mater. Sci. 189 (2021) 110251.
[29] D. Kong, K. Liu, Z. Wang, Hyperbolic mean curvature flow: evolution of plane curves, Acta Math. Sci. 29B (3) (2009) 493–513.
[30] D.-X. Kong, Z.-G. Wang, Formation of singularities in the motion of plane curves under hyperbolic mean curvature flow, J. Differ. Equ. 247 (6) (2009) 1694–1719.
[31] V. Kusumasari, Hyperbolic mean curvature flow with an obstacle, Sci. Rep. Kanazawa Univ. 62 (2018) 1–22.
[32] P.G. LeFloch, K. Smoczyk, The hyperbolic mean curvature flow, J. Math. Pures Appl. 90 (6) (2008) 591–614.
[33] J. Mao, Forced hyperbolic mean curvature flow, Kodai Math. J. 35 (3) (2012) 500–522.
[34] J. Mao, C.-X. Wu, Z. Zhou, Hyperbolic inverse mean curvature flow, Czechoslov. Math. J. 70 (1) (2020) 33–66.
[35] J.A. McCoy, I. Otuf, Representation formulae for linear hyperbolic curvature flows, J. Differ. Equ. 397 (2024) 166–198.
[36] V. Minárik, M. Beneš, J. Kratochvíl, Simulation of dynamical interaction between dislocations and dipolar loops, J. Appl. Phys. 107 (2010) 061802.
[37] P. Pauš, M. Beneš, M. Kolář, J. Kratochvíl, Dynamics of dislocations described as evolving curves interacting with obstacles, Model. Simul. Mater. Sci. Eng. 24 (3) (2016) 035003.
[38] P. Pauš, M. Beneš, Direct approach to mean-curvature flow with topological changes, Kybernetika 45 (4) (2009) 591–604.
[39] L. Pontryagin, Ordinary Differential Equations, Nauka, Moscow, 1965.
[40] H.G. Rotstein, S. Brandon, A. Novick-Cohen, Hyperbolic flow by mean curvature, J. Cryst. Growth 198/199 (1999) 1256–1261.
[41] H.G. Rotstein, A. Nepomnyashchy, A. Novick-Cohen, Hyperbolic non-conserved phase field equations, J. Cryst. Growth 198/199 (1999) 1262–1266.
[42] D. Ševčovič, S. Yazaki, Computational and qualitative aspects of motion of plane curves with a curvature adjusted tangential velocity, Math. Methods Appl. Sci. 35 (15) (2012) 1784–1798.
[43] P. Strachota, A. Wodecki, High resolution 3D phase field simulations of single crystal and polycrystalline solidification, Acta Phys. Pol. A 134 (3) (2018) 653–657.
[44] M. Suchomelová, Evolution equations for planar curves and their generalization, Diploma Project in Mathematical Engineering, Faculty of Nuclear Sciences and Physical Engineering, Czech Technical University in Prague, June 2022.
[45] Z. Wang, Hyperbolic mean curvature flow in Minkowski space, Nonlinear Anal., Theory Methods Appl. 94 (2014) 259–271.
[46] Z. Wang, Hyperbolic mean curvature flow with a forcing term: evolution of plane curves, Nonlinear Anal., Theory Methods Appl. 97 (2014) 65–82.
[47] Z. Wang, Symmetries and solutions of hyperbolic mean curvature flow with a constant forcing term, Appl. Math. Comput. 235 (2014) 560–566.
[48] Z. Wang, R. Ding, Hyperbolic inverse mean curvature flow with forced term: evolution of plane curves, Math. Methods Appl. Sci. 46 (6) (2023) 6660–6673.
[49] Z. Wang, S. Lv, B. Zhao, Dissipative hyperbolic mean curvature flow for closed convex plane curves, J. Funct. Anal. 285 (5) (2023) 110023.
[50] W. Wo, F. Ma, C. Qu, A hyperbolic-type affine invariant curve flow, Commun. Anal. Geom. 22 (2) (2014) 219–245.
[51] S.-T. Yau, Review of geometry and analysis, Asian J. Math. 4 (1) (March 2000) 235–278.
[52] Z. Zhou, C.-X. Wu, J. Mao, Hyperbolic curve flows in the plane, J. Inequal. Appl. (2019) 52.